46th AIAA Aerospace Sciences Meeting and Exhibit
7 - 10 January 2008, Reno, Nevada

AIAA 2008-300

Aerodynamic Performance Enhancement of a NACA 66-206 Airfoil Using Supersonic Channel Airfoil Design

David M. Giles[1] and David D. Marshall[2]
California Polytechnic State University, San Luis Obispo, CA, 93407-0352

Supersonic channel airfoil design techniques have been shown to significantly reduce drag in high-speed flows over diamond shaped airfoils by Ruffin and colleagues. The effect of applying these techniques to a NACA 66-206 airfoil is presented. The design domain entails channel heights of 8-16.6% thickness-to-chord and speeds from Mach 1.5-3.0. Numerical simulations show an increase in the lift-to-drag ratio for airfoils at Mach 2.5 at a 35,000-ft altitude with a 12% channel height geometry showing a benefit of 17.2% at 6-deg angle of attack and a sharp channel leading edge. Wave drag is significantly reduced while viscous forces are slightly increased because of greater wetted area. Lift forces compared to clean airfoil solutions were also decreased, due mainly to the reduction in the length of the lifting surfaces. A tensile yield failure structural analysis of a typical beam found an 11.4% channel height could be implemented over 50% of the span between two typical ribs. A three dimensional wing was designed with the determined slot geometry and two dimensional flow analyses. An overall increase in L/D of 9% was realized at Mach 2.5 at a 35,000-ft altitude and 6-deg angle of attack.

Nomenclature

C_p	=	pressure coefficient
c	=	chord (m)
L/D	=	Lift-to-Drag ratio
R	=	Rounded Leading Edge
R_n	=	Nose Lip Radius (mm)
t_c	=	Channel Thickness (mm)
S	=	Sharp Leading Edge
θ	=	Channel Half Angle (degrees)
y^+	=	Non-Dimensional Turbulent Length Scale
α	=	angle of attack (degrees)

I. Introduction

TAILORING the aerodynamic performance of a high speed aircraft such as a supersonic civil transport towards cruise conditions can optimize criteria such as range, fuel fraction, and payload. By maximizing L/D many of these performance parameters can be improved. However, to reach supersonic speeds, a self-propelled aircraft must traverse both the subsonic and transonic regimes. Many airfoils designed only for supersonic cruise performance, such as a diamond airfoil, have very low lifting characteristics at slow speeds. To counteract this, in some designs cambered airfoils are used in some sections of the wing to provide lift for subsonic operation. In supersonic flight, this cambered and often blunted nose airfoil section has a lower L/D because of the high wave drag associated with the stagnation point.

In previous work[1,2] blunted diamond airfoils were examined to improve drag characteristics. A sharp leading edge airfoil is hard to construct and suffers from high heat transfer rates at high supersonic speeds. However, blunting the leading edge causes a large increase in the wave drag of the aircraft because of the large stagnation pressure point. To decrease the wave drag during cruise, a channel opens up in the middle of the airfoil and split the large stagnation region into two smaller points. If the channel height is sufficiently small to choke the flow entering

[1] M.S. Candidate, Aerospace Engineering Department, Student Member.
[2] Assistant Professor, Aerospace Engineering Department, Senior Member.

the channel, a bow shock will form in front of the airfoil and the flow traveling through the channel will be subsonic, and thus have a lower dynamic pressure. The greater wetted area does increase the skin-friction drag, but the subsonic flow in the channel minimizes this increase. By implementing a channel through the wing, the overall drag was reduced by up to 20% for some geometries in turbulent flow. Further work included experimentation in reducing heat transfer rates due to hypersonic velocities by rounding off the two nose lips caused by the channel geometry[3]. By using an appropriate channel design the cruise efficiency of a wing can be increased or the wing sweep can reduced for the same aerodynamic benefit.

The present concept applies this previous work to a cambered airfoil, specifically a NACA 66-206 with a chord length of 1 m. The channel begins at the leading edge, extends through the airfoil, and exits at the trailing edge. The initial channel heights range from 8% to 16.6% of the total thickness with the center of each channel at the zero angle stagnation point of the airfoil. The resultant leading edges are rounded to a 3 mm radius to promote easier construction and to decrease heat transfer if placed in supersonic flow as seen in Figure 1. Sharp leading edge geometries were also constructed since at lower supersonic cruise speeds, the effects of heat transfer are not as severe. The channel extends through the airfoil, enlarging at a half angle of 0.05 degrees to account for boundary layer growth in the channel. The trailing edge location is determined by the location that has a thickness that corresponds to the height of the channel at that chord. This does not guarantee a straight channel because of the cusped section on the lower surface. Instead, the centerline of the channel extends straight back to 0.15c, turns up at a slight angle to 0.75c, and continues to extend straight out the trailing edge. These locations were chosen as they correspond to typical spar locations to be used in the structural analysis portion of this study.

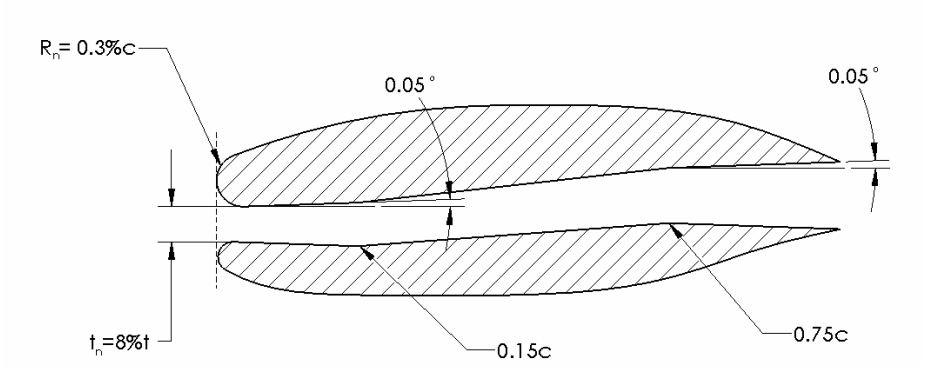

Figure 1. Geometry for 8% Channel NACA 66-206 Airfoil (Not to Scale)

A disadvantage to using a non-symmetric airfoil compared to a blunted diamond airfoil is the straight trailing edge geometry in the non-symmetric section. When a channel is carved out, large amounts of geometry are removed. For the 16.6% rounded channel, the overall chord length was reduced to 0.89c. When the sharp channel is used, about 1% of the chord length was recovered to act as a lifting surface. A blunted diamond airfoil loses little of its internal volume as long as the channel height does not exceed the blunted nose radius.

II. Numerical Results: 2D Computational Fluid Dynamics

The basic geometry utilized was adapted from the inboard section of a reference high speed supersonic transport having a cranked arrow type design[4]. Initial grid sizes constructed using GAMBIT[5] contained approximately 25,000 cells in the 2D plane. A modified C-grid was used to set the farfield boundaries. Structured grids using quad elements were used in all locations except directly in front of the channel where a pave-type quad mesh was implemented. To ensure viscous effects could be captured, the first node was placed at .0014c from the surface, giving an initial y^+ value from 100-250 which set the initial cell within the log layer. Within the channel, six cells were used per chord station to keep the cells as orthogonal as possible around the leading edge.

Turbulent flow analysis was predicted using a k-ω viscous model in Fluent[6]. Gradient adaptation was implemented for pressure gradients to ensure an accurate capture of the bow shock and oblique shocks near the trailing edge. Also, grid adaptation was used to refine the boundary layer to have maximum y^+ value of 100 to capture the viscous effects. The final adapted grids for the 10% channel and the no channel airfoil can be seen in Figure 2. Both grids captured the bow shock and the trailing edge shocks similarly.

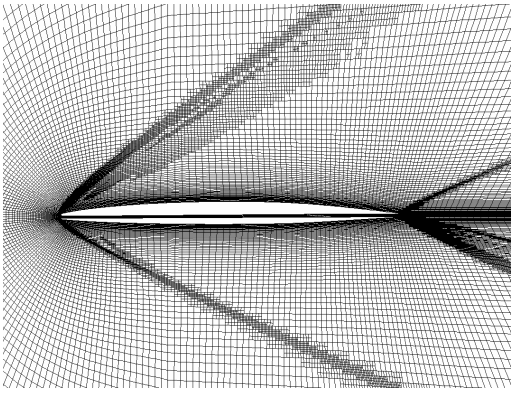

Figure 2a. Adapted Grid for Channel Thickness of 10% at M_∞ = 2.5

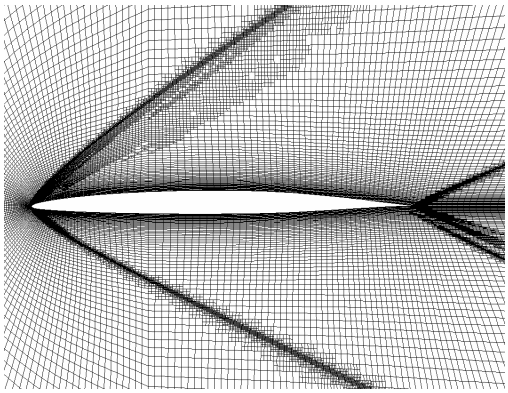

Figure 2b. Adapted Grid for NACA 66-206 with No Channel at M_∞ = 2.5

The five channel geometries examined were 8%, 10%, 11.4%, 12%, and 16.6% of the total t/c of the airfoil. Rounded channel lips were examined first. Initial results of the 8% airfoil at M_∞= 2.5 showed no decrease in the drag coefficient and so larger channel geometries were examined. With the 16.6% channel, a decrease in the drag coefficient was seen. Note that all coefficients are non-dimensionalized by the actual airfoil chord length for each geometry.

After initial data had been obtained, a coarse sweep over a range of Mach numbers was obtained at an angle-of-attack of 6° to ensure a positive lift force was obtained. Also, the effect of implementing a sharp leading edge to the channel entrance was also examined in this sweep. The Mach contours for the M_∞= 2.5, 35,000 ft altitude case for three geometries can be seen in Figure 3. All three had similar external flow fields, even at the trailing edge, where a similar contour of oblique shocks and expansion waves were present. The flow for the rounded channel cases was choked and a bow shock formed in front of the leading edge of the airfoil, with a comparable location to the baseline airfoil. Internally, the flow was subsonic until the channel exit where it became sonic. This was desired in order to keep the viscous drag as low as possible. At the exit the flow reached Mach 1. The sharp leading edge channel also was choked, but not at the entrance. Instead a started inlet condition existed with oblique shocks and expansions. After the flow had slowed to subsonic, the airflow accelerated and at the exit of the channel reached Mach 1.

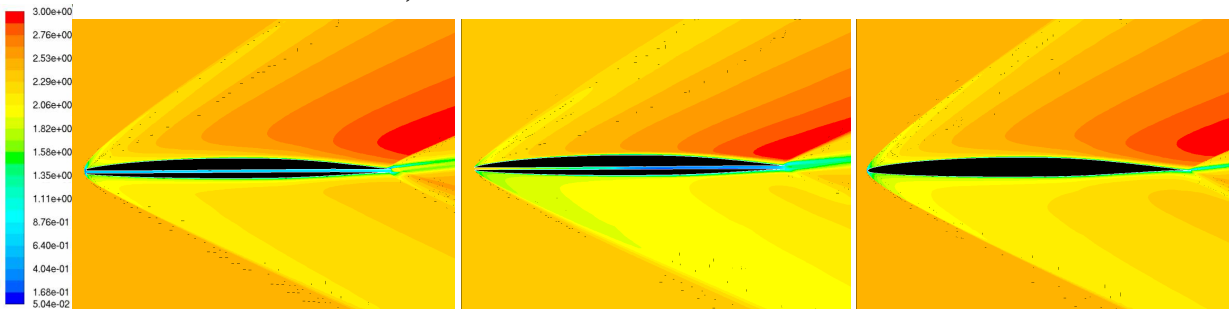

Figure 3. Mach Contours for a) 12% thick round channel b) 12% thick sharp channel and c) baseline airfoil at M_∞= 2.5, 35,000 ft altitude, and α = 6°.

A full bow shock formation for a rounded leading edge channel can be seen in Figure 4a. Because the flow is choked near the trailing edge, the subsonic region is present in the channel towards the leading edge. At the leading edge lips, two small stagnation regions form their own bow shocks. If the channel opening is sufficiently small, these tow shocks can interact along with the choked channel to form a continuous bow shock in front of the leading edge. For small channels, the bow shock is round in the front. In the 12% case shown, the shock has a flat section in front of the channel. This was due to the bow shock regions associated with each lip having smaller interactions, causing a weaker area directly in font of the channel. For each rounded case examined in this effort, the bow shock was present. The sharp leading edge airfoil geometry provided a much different flow field at the leading edge. Figure 4b shows how the two shock regions are unable to form a continuous bow shock over the front of the channel. Instead, oblique shocks and expansion waves are present in the channel. The stagnation pressure regions

are smaller than that of the rounded channel. The supersonic flow in the channel does increase the amount of viscous drag but the sharp leading edge decreases the wave drag seen by the airfoil.

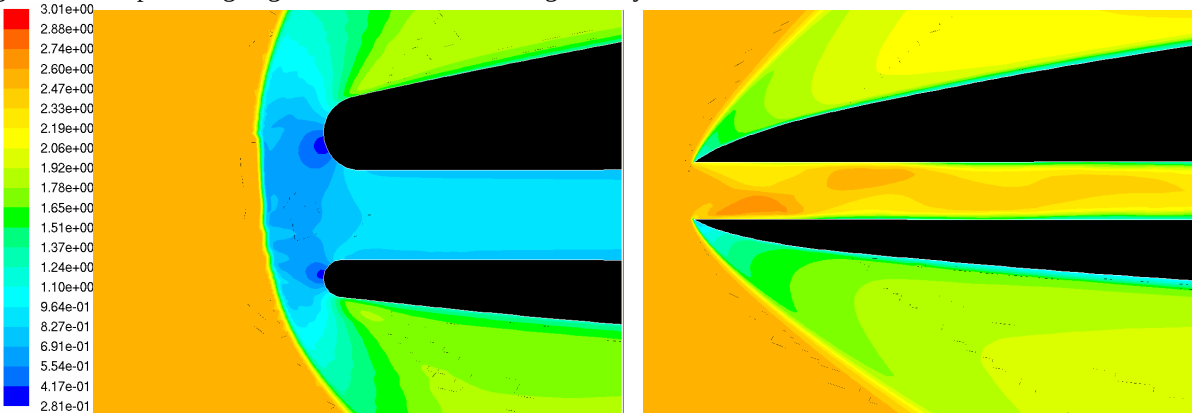

Figure 4. Leading Edge Mach Contours for a) 12% thick round channel and b) 11.4% thick sharp at M_∞= 2.5, 35,000 ft altitude, and α = 6°.

The large stagnation point on the baseline airfoil was split into two points for the channel airfoil. The magnitude of the pressure coefficient (C_p) was about 1.7 in all M_∞= 2.0 cases. However, the high pressure region was much smaller for the channel cases. The sharper decrease in a C_p for the channels when compared to the baseline airfoil can be seen in Figure 5. The channel design exhibits similar trends over the external surfaces of the airfoil as the baseline airfoil. No lift was produced from the channel because of the balance of the pressure forces, easily seen in the graph as the two faces are the same distribution. The irregularity for the 16.6% channel was caused by the flow starting to accelerate to sonic speeds inside of the channel. The pressure data from inside the channel will be used in the structural analysis.

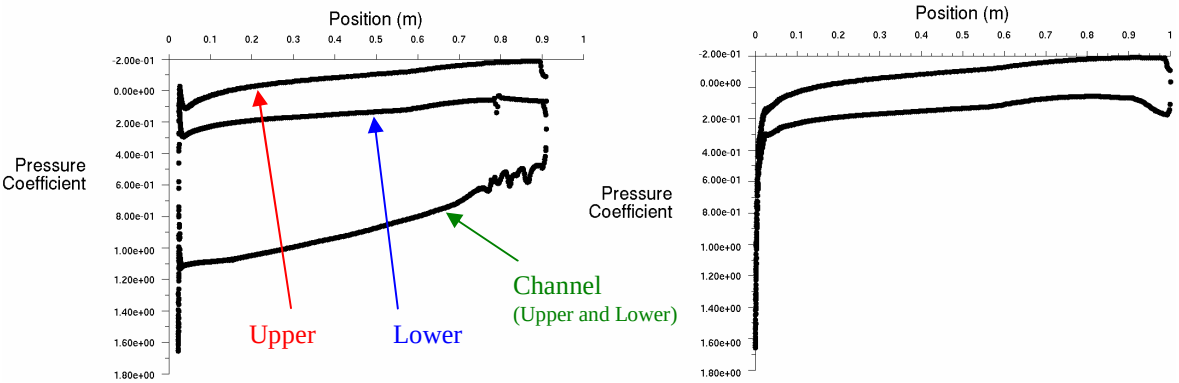

Figure 5. Pressure Coefficient Distributions on Exposed Surfaces for a) 16.6% thick channel and b) baseline airfoil at M_∞= 2.0, 35,000 ft altitude, and α = 6°.

When compared to the baseline airfoil, all channel airfoils had an increase in viscous drag. For the M_∞= 2.5 cases, the viscous drag of about 600 N/m for the channel airfoils was double that of baseline (321 N/m). This doubling trend was observed in all rounded leading edge case except when speed decreased to a freestream Mach of 1.5 where the drag only increased by a factor of 1.6 (171 N/m to 282 N/m).

Table 1 shows the benefit seen in both the sharp leading edge and rounded leading edge at the Mach 2.5 and six degree angle of attack condition. As expected, the pressure drag force was decreased because the large stagnation region caused by the bow shock was dissipated into two smaller stagnation points. The decrease was about 17% for the rounded 12% channel airfoil. The wave drag was reduced more than the viscous drag increased, causing the overall drag force on the airfoil to be less. The greatest benefit was seen by the sharp leading geometry. Because of the smaller stagnation region, the wave drag was reduced by 34% for the 12% airfoil when compared to the baseline. The viscous drag increased by 25% over the rounded channel airfoil because of the supersonic flow present at the inlet of the channel. At M_∞= 2.5, the wave drag magnitude was approximately four times greater than the viscous drag. The decrease in pressure drag overcame the increase in viscous drag to lower the overall drag on the airfoil by

21% compared to the baseline NACA 66-206. Overall it was seen that for a supersonic channel airfoil, even for the rounded channel, the small penalty for increased viscous drag can be reversed by the decrease in wave drag significantly, especially at higher Mach numbers.

Table 1. Two Dimensional Performance Results for Mach 2.5, 35,000ft, α = 6°

	Drag Force (N/m)			Lift Force (N/m)		
CaseName	Pressure	Viscous	Total	Pressure	Viscous	Total
12% Sharp	2616	778	3394	16481	-75	16407
12% Round	3313	620	3933	15637	-60	15578
Baseline	3990	321	4311	17805	-30	17775

In order to normalize all geometries, L/D was examined and the results can be seen in Figure 6. Even though the drag forces were much lower on the channel airfoils, the lift forces were also decreased. By eliminating part of the trailing edge geometry to implement the channel, up to 11% of the no channel airfoil lifting surface was also eliminated. At lower Mach numbers this did not have as great of an effect, but at high Mach numbers, the disparity between the baseline airfoil and the rounded channel airfoil lift forces was on the order of a few kilonewtons. An increase in L/D was seen for 16.6% channel at Mach 2.0, which is a reasonable cruise speed. If the cruise speed was decreased to Mach 1.5, all channel airfoils examined outperformed the baseline airfoil. The maximum increase in L/D for a rounded leading edge airfoil was 3.5% for the 16.6% channel airfoil. When the sharp leading edge was implemented, the increase in L/D was much more apparent. At Mach 2.5, the L/D increase was 17.2% for the 12% airfoil. A larger decrease in the wave drag overcame a slight increase in the viscous drag. Also, the sharp geometry recovered some of the chord length at the leading edge, allowing for a larger lifting surface. This gave higher lift values for the sharp leading edge geometry compared to the rounded leading edge. For the 12% case, 5.3% more lift was realized as seen previously in Table 1. The lift produced was still lower than the baseline airfoil which had a full chord length. At higher speeds, the losses in lift were greater than at the slower supersonic speeds. The longer chord length of the sharp channel and the lower drag from the lip geometry allowed for more efficient cruise over both the baseline and rounded leading edge channeled airfoils as long as the sharp leading edge could overcome structural and thermal impediments.

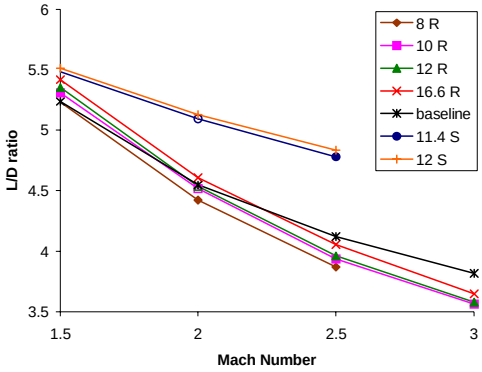

Figure 6. Computed L/D for Various Mach Numbers; α = 6° and altitude = 35,000 ft

The channel geometry was also examined to try and improve the performance by obtaining a propulsive force out of the high pressure air in the channel. Two channels were created that started with an 8% channel at the inlet and the exit as a 16.6% channel. One channel had the normal two kink configuration at the spar locations and the other had a straight channel edges from the 8% inlet to the 16.6% outlet. The number of kinks in the channel only caused a difference in L/D of 0.2%, which could be attributed to the coarseness of the grid. Overall, the growth of the channel gave the effect of a diverging nozzle because the expansion was much greater than the 0.1° used for a normal channel. However, since the flow exit was much larger than the inlet, the flow did not choke at the end of the channel but at the narrowest point of the channel, the inlet point of the channel as seen in Figure 7. This caused supersonic flow throughout the entire length of the duct. The bow shock structure correlated with a constant channel height of 8%. The viscous drag was similar in magnitude to an 8% channel, but the pressure drag did decrease when compared to an 8% channel. The pressure in the channel

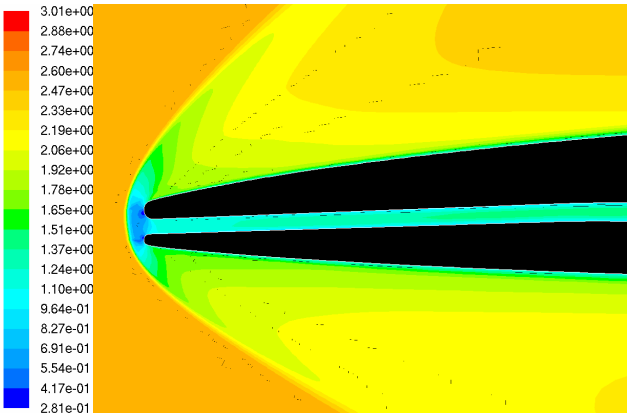

Figure 7. Leading Edge Mach Contours for Diverging Channel (8% to 16.6%) at M_∞= 2.5, 35,000 ft altitude, and α = 6°.

acted on the interior walls of the channel, overcoming a portion of the stagnation pressure. The overall drag was similar to that of an 11% channel. The decrease in lifting surface because of the large exit of the channel hindered the performance of the airfoil. The overall L/D was 3.84 which was less than the 3.86 for a typical 8% channel.

III. Numerical Results: Structural Analysis

A basic structural analysis was performed to determine the allowable width of the channel due to the cut needed through the spars of an aircraft. PanAir[9], a panel code, was used to approximate the loading the wing would incur during Mach 2.5 flight. Using the wing planform from the reference aircraft[4], the resultant lift distribution was determined using the doublet strength at the trailing edge. Given a 665,000 lb base cruise weight for the aircraft[8], the forces on the wing were determined. A chord length of 7.024m was determined by the halfway point of the outboard section of the cranked arrow design. This chord translated into a 0.298m high spar for the 0.15c spar. The forces present at the end of spar width, where a rib would attach, were a moment of 14,534 Nm and a vertical point load of 2,075 N determined from the air load analysis. The material chosen was Aluminum 2024-T4[10], a typical aircraft aluminum with a tensile yield strength of 3.25×10^8 Pa. An I-Beam profile was optimized for the loading and tensile limits of the material given the constraints of 0.002 m for the web and 0.003 m for the flange. An untapered spar was constructed from the I-beam profile and the stress profile of the beam in the loaded condition can be seen in Figure 8. In the finite element model constructed, the maximum stress computed was 3.18×10^8 Pa and this value was used as the failure criterion in further analyses.

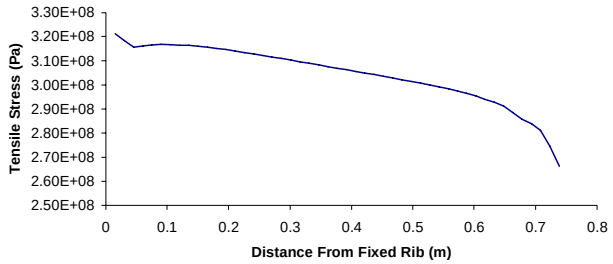

Figure 8. Stress Profile for 0.15c I-Beam, no cutout

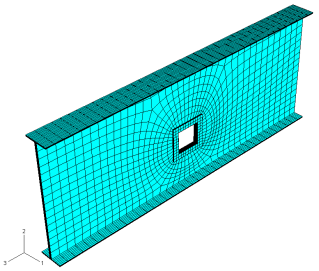

Figure 9. Grid for Reinforced Square Cutout

The grid used was seeded using evenly spaced grid points. Quadrilateral solid elements were used. The cutout location was based on the location given from the airfoil for both 0.15c and 0.75c spar locations. The grid was structured except around the cutouts for the channel. A paver mesh was used and the results for a square cutout can be seen in Figure 9. The material carved away to make room for the hole through the spar was added around the hole, reinforcing the web section of the spar and also providing a location for a duct structure to attach.

Initial studies on circular channels found that the 0.15c spar was more limiting than the 0.75c for all channel sizes. The next study focused on the 12% channel by changing the span of the cutout and reinforcing the area around the cutout. Besides the square geometry seen above, slot geometries with semi-circle close outs to eliminate the sharp stress concentration of the square geometry were implemented. The results were computed for slots up to 50% of the span of the spar and a summary of the data is seen in Table 2. When material was eliminated the peak stress was up to 6% higher than the reinforced hole geometry. However, all slots still failed the tensile yield failure criterion. However, by altering the geometry and not adding any material, the stress was decreased. The next approach was to alter the taper of the flanges which were originally the same cross section throughout the length of the spar model. After analyzing the results of both 10% and 12% spar geometries, the final taper geometry and channel sizing of 11.4% was determined and was shown in Figure 10. The stress profile is seen in Figure 11 and was similar to the other slot models by having two stress peaks near the ends of the slot. As predicted from the trends observed in the previous models, the 11.4% model optimally met the 3.18×10^8 Pa tensile yield failure criterion.

Table 2. Maximum Tensile Stress (Pa) with Slotted I-Beam

Slot Size	Normal Cutout	Reinforced Hole
Square	3.30E+08	3.22E+08
25%	3.42E+08	3.27E+08
50%	3.50E+08	3.29E+08

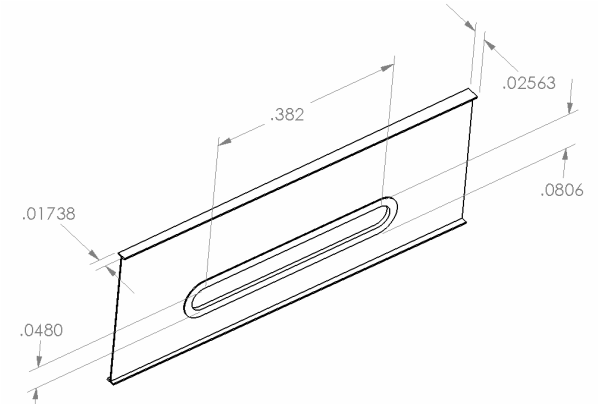

Figure 10. 50% Slotted Beam Geometry, 11.4% Channel Height (m)

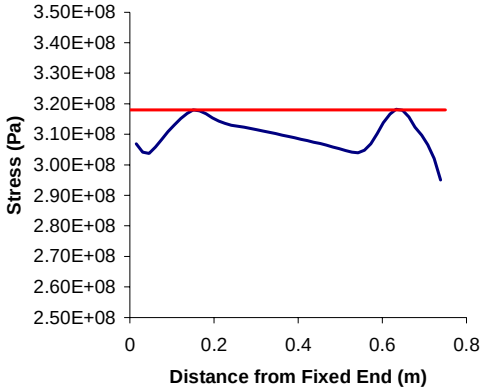

Figure 11. Stress Profile for 11.4% Channel Height 50% wide slot

The pressure force due to the air through the duct was also taken into consideration. When added into the structural model, the tensile stress increased a maximum of 1%. The pressure load may be critical to other structural failure modes, but since the effect on the tensile yield was small, further analysis was done without the interior pressure loading.

IV. Numerical Results: 3D Computational Fluid Dynamics

A three dimensional model was created that coupled the results of the previous analyses by implementing a sharp leading edge slotted channel that was 11.4% high and covered 50% of the span between two ribs. The model used symmetry planes at the span rib location and also at the span location at the center of the channel. A baseline 3D model was also created with the symmetry planes were modeled at the two rib locations. The full solid model constructed can be seen in Figure 12. The gridding scheme used was similar to the two dimensional models. The rib symmetry plane was meshed the same as the normal baseline airfoil. The profile at the center of the slot matched 2D profile with a channel and was gridded similarly. The flow field was then meshed with mapped hexahedral elements. During the flow solution computation, gradient adaptation was implemented again for pressure gradients to ensure an accurate capture of the leading edge flow characteristics and the oblique shocks near the trailing edge. A maximum of two levels of refinement were used.

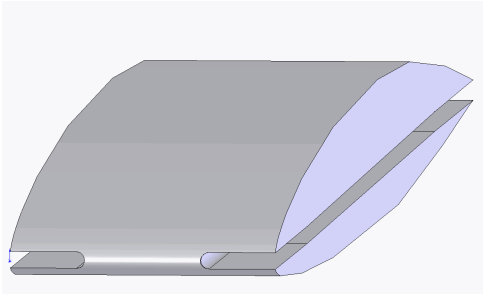

Figure 12. Model Geometry for Slotted Wing

The two wing models were subject to Mach 2.5 flow at a standard altitude of 35,000 ft and six degrees angle of attack. The slotted wing showed an L/D improvement of 9.2% over the baseline model with an L/D of 4.48 as shown in Table 3. In the table, the forces on the slotted wing geometry were doubled since it was a half model. The drag force was reduced by 64 N and the lift force was decreased as well by 108 N. The reduction in lift was followed what had been seen in the airfoil section analysis. The reduction was 5.5% for the entire model. This was similar to the 11.4% section airfoil which had a reduction of 6.9%. The discrepancy was expected because some of the slotted wing was not altered and had a full airfoil section and from this some of the lift force was recovered when compared to a fully slotted wing.

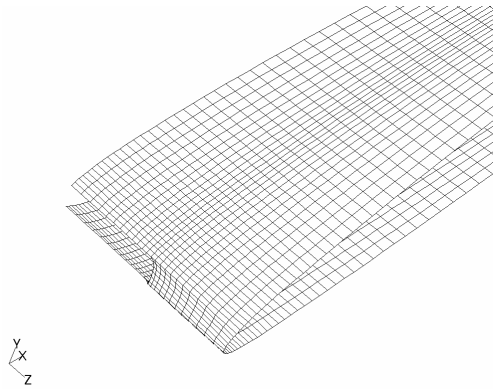

Figure 13. Surface Mesh of Slotted Geometry (Half Model)

The two dimensional baseline results were also scaled based on the 3D baseline model which had a width of .109c. For a fully slotted wing, the expected L/D value was 4.78 and using the

baseline wing model, 4.102. The slotted wing had a performance that was 56% of this range even though the slot was only 50% of the wing. This increase is reasonable since the total slot did not only cover 50% of the wing leading edge. The circular close off of the slot went beyond the 50% slot allotment. This extra cutout was included in the structural model previously. This extra frontal area reduced the drag further since the channel was open to more of the span. The amount of benefit was reduced when compared to an 11.4% slot extended because the diminishing size of the close off. The benefit was not large but was apparent.

Table 3. Comparison of Baseline and Channel Airfoils and Wings for Mach 2.5, 35,000 ft, α = 6°, Force Data Scaled to Baseline 3D model.

	Drag Force (N)			Lift Force (N)			
CaseName	Pressure	Viscous	Total	Pressure	Viscous	Total	L/D
Baseline 3D	436	36	472	1941	-3	1938	4.102
50% Slot 3D	350	58	408	1832	-6	1828	4.480
Baseline 2D	434	35	469	1937	-3	1933	4.123
11.4% Channel 2D	297	80	376	1806	-8	1799	4.780

The external surfaces of the leading edge affected the performance of the airfoil downstream. A pressure plot of the leading edge can be seen in Figure 14. The large stagnation region caused by the full airfoil can be seen. In contrast, the slotted section has a much smaller stagnation region. Where the slot section ends, there was no longer a surface to support the bow shock flow feature and the flow collapsed into the channel. The interaction is seen on the lips of the channel. For most of the leading edge of the slot, the stagnation region was small and was parallel to the leading edge. At the point where the bow shock at the edge of the channel close out interacted with the lips of the slot, a high pressure region developed. Also interacting at this point was the shock that was developed by the sharp edged lips of the channel itself. From this region, the propagation of a shock wave caused by this discontinuity continued along the surface of the wing, interacting with the accelerating flow over the top of the wing. The propagation of the discontinuity can also bee seen on the interior surfaces of the channel.

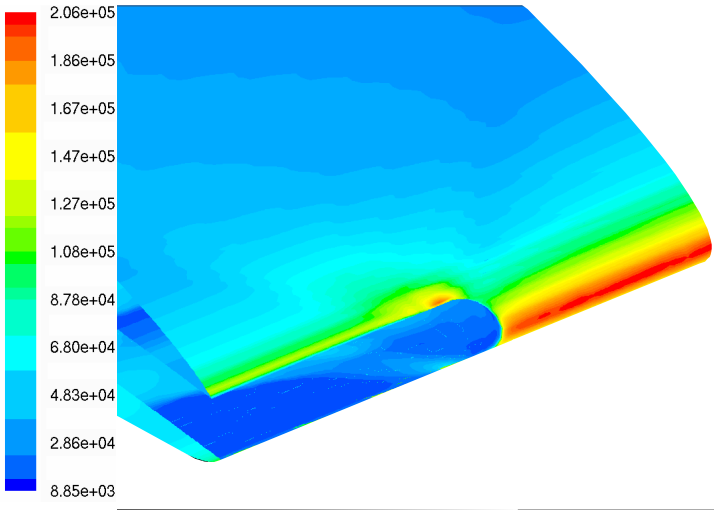

Figure 14. Pressure Contours (Pa) of Leading Edge Surfaces for 11.4% Channel, 50% width at Mach 2.5, 35,000 ft, α = 6°

The flowfield varied for the slotted wing depending on the span location. Figure 15 shows the flowfield along the slot symmetry line. Overall, the flow characteristics were similar to that of the airfoil section with an 11.4% channel. Leading edge shocks form at the lips of the channel and the bow shock region was not formed as expected. The trailing edge also was similar, with the flow expanding out the exit of the channel and accelerating past sonic. However, because of the finite nature of the slot other elements came into play. Instead of a continuous acceleration over the upper surface, the flow was interrupted by the shock formed by the discontinuity interacting with the accelerating flow over the top of the wing. The formation of this shock and its interaction along the symmetric boundary could have contributed to some of the drag seen by the wing.

The overall flow through the channel was comparable to the basic channel airfoil. Because of the boundary conditions present, the flow field was altered from the infinite channel. The centerline of the channel coincided closely to that of the slotted airfoil section model. Near the leading edge, a supersonic zone was found with both expansion waves and oblique shocks interacting. The zone eventually coalesced and became a subsonic flow at about 0.25c as seen in Figure 16. The flow stayed near sonic until the trailing edge, where the flow sped up back to supersonic speeds at the exit of the channel. Near the slot close out boundary, the flow did differ from the performance seen in the 11.4% slotted airfoil. At the leading edge, the discontinuity caused by the closeout of the slotted propagated a shock into the channel as well as the upper and lower surfaces of the airfoil. The initial region

of the channel is highly convoluted as shocks generated from the upper and lower lips as well as the close out regions all interact. At about 0.05c from the leading edge, the boundary layer, which had been attached, was tripped by a wave hitting the sides of the slot. A separated region was developed after this perturbation of the boundary layer. Further down the slot, the flow became more uniform and the separation region was damped out. Since the inviscid region of the channel was smaller than usual in the front, the flow was able to expand more in the aft region of the channel. This allowed the flow to be slower in this section, only Mach 0.7, whereas in the infinite channel, the flow was near sonic or parts of the flow were expanding past Mach 1. This lower velocity allowed for less viscous drag in this part of the channel compared to the two dimensional model. This offset the drag increase caused by the separation region near the front of the channel. At the exit of the channel, the choked flow expanded and accelerated, similarly to that of the two dimensional model. The interaction of the channel and the trailing edge portion of the airfoil had no large irregularities except oblique shocks and expansion waves to match the flow from both external and internal surfaces which was similar to that in the two dimensional analysis.

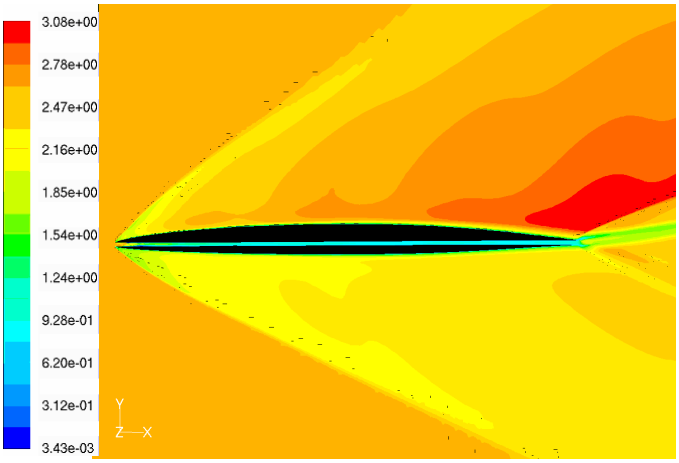

Figure 15. Mach Contours for Mid-Plane Section of 3D Channel

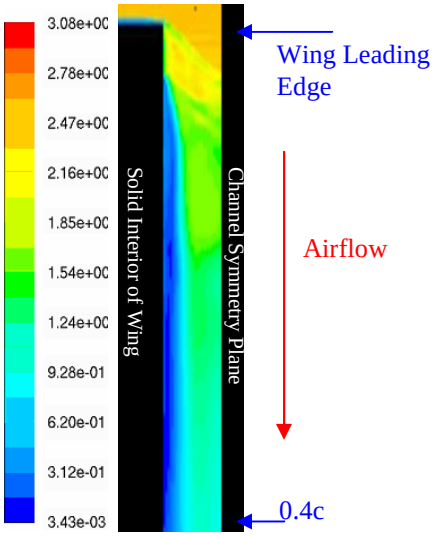

Figure 16. Contours of Mach Number for 11.4% Channel Symmetry Plane for Mach 2.5, 35,000 ft, α = 6°

V. Conclusions

The supersonic channel airfoil concept was applied to an airfoil that was not solely designed for supersonic cruise, specifically a NACA 66-206 airfoil. Initial two dimensional results showed an increase in L/D for the airfoil with the supersonic channel implemented. The structural implications were also examined. It was found that a baseline beam could be altered to accommodate a 50% slot through the spar. The failure mode of tensile yielding was not affected by the internal pressure of the air flowing through the channel. Finally, an aerodynamic analysis of the wing structure was performed. The experiment showed an increase in the L/D of 9% for a wing with an 11.4% t/c supersonic channel height implemented over 50% of the span between to ribs. The wing examined was an infinite rectangular wing subject to conditions at Mach 2.5 at six degrees angle of attack and placed in a standard altitude condition of 35,000 ft.

The implementation of the channel still requires further refinement. The current design would have the channel be opened during cruise so subsonic maneuvering would use the full NACA 66-206 profile. This is especially needed for the sharp leading edge channel concept. Also, the elimination of area at the trailing edge lowered the lift force generated by the wing, negating some of the performance gained by the drag reduction. Other airfoils may be more suited to the channel concept. Additionally, the structural analysis was limited to a basic analysis in order get a first iteration of the feasibility of this concept. More work needs to be done to investigate how this could be applied to an actual structure. Further analysis into structural penalties for ducting structure, heat transfer, and actuation of the channel are needed.

The improvement in L/D performance for a wing during cruise can be applied in many ways. The most basic is a straight implementation into a current design wing profile that would allow a higher L/D of the aircraft to occur. Another application is the reduction of the sweep to make the L/D performance with the supersonic channel to be the same as the baseline wing footprint. The reduction in sweep will allow for greater performance for subsonic

operations. Overall, the use of a blunt airfoil on a wing for subsonic performance enhancement does not have to add as large of a penalty during supersonic flight because the application of the supersonic channel airfoil design will provide a means to decrease fuel costs, increase range, and increase payload while not compromising the subsonic performance of the aircraft.

Acknowledgements

The author would like to thank Dr. Peter Schuster for his support for the structural analysis portion as well as Dr. Stephen Ruffin for providing valuable feedback on this research.

References

[1]Ruffin, S., and Gupta, A., "Supersonic Channel Airfoils for Reduced Drag," AIAA Paper 97-0517, Jan. 1997.

[2]Ruffin, S., Gupta, A., and Marshall, D., "Supersonic Channel Airfoils for Reduced Drag," *AIAA Journal*, Vol. 38, No. 3, 2000, pp. 480-486.

[3]Gupta, A, and Ruffin S., "Optimal Artificially Blunted Leading-Edge Airfoils for Enhanced Aerothermodynamic Performance," *Journal of Spacecraft and Rockets*, Vol. 36, No. 4, Jul. 1999, pp. 499-506.

[4]Rinoie, K., and Miyata, K., "Studies on Vortex Flaps with Rounded Leading Edges for Supersonic Transport Configuration," *Journal of Aircraft*, Vol. 41, No. 4, Jul. 2004, pg 830.

[5]GAMBIT, Ver. 2.2.30, Fluent, Inc, 2006.

[6]Fluent, Ver. 6.2.16, Fluent, Inc, 2005.

[7]Gupta, A, and Ruffin S., "Aerothermodynamic Performance Enhancement of Sphere-Cones Using the Artificially Blunted Leading-Edge Concept," *Journal of Spacecraft and Rockets*, Vol. 37, No. 2, Mar. 2000, pp. 235-241.

[8]Wright, B. R., Bruckman, F., and Radovcich, N.A., "Arrow Wings for Supersonic Cruise Aircraft," *Journal of Aircraft*, Vol. 15, No. 12, Dec. 1978, pp. 829-836.

[9]PanAir, 1992

[10]Beer, Ferdinand P., Johnston, Jr, E. Russell, DeWolf, John T., Mechanics of Materials, 3rd Edition, 2002, pp.747.